

# Numerical Simulations of Magnetoplasmadynamic Thrusters with Coaxial Applied Magnetic Field

IEPC-2007-138

*Presented at the 30<sup>th</sup> International Electric Propulsion Conference, Florence, Italy  
September 17-20, 2007*

Daniel Haag\*, Markus Fertig†

*Universität Stuttgart, Institut für Raumfahrtsysteme, Pfaffenwaldring 31, 70569 Stuttgart, Germany*

and Monika Auweter-Kurtz‡

*Universität Hamburg, Edmund-Siemers-Allee 1, 20146 Hamburg, Germany*

An overview is given on a numerical simulation program for applied field magnetoplasmadynamic (AF-MPD) thrusters, which is currently under development at the Institute of Space Systems (IRS). The program allows the simulation of argon plasma flows under thermal and chemical non-equilibrium. The code is based on an axisymmetric finite volume method on unstructured, adaptive meshes. An externally applied magnetic field can be taken into account employing the vector potential formulation. Azimuthal velocity and magnetic field are handled by a quasi-three dimensional approach with vanishing azimuthal derivatives.

## Nomenclature

$\Delta A$	Finite volume cell area [m <sup>2</sup> ]
$\vec{A}$	Vector potential [Vsm <sup>-1</sup> ]
$\vec{B}$	Magnetic induction [T]
$D_{im}$	Effective diffusion coefficient of heavy particle species $i$ [m <sup>2</sup> s]
$\vec{E}$	Electric field [Vm <sup>-1</sup> ]
$e$	Energy density [Jm <sup>-3</sup> ]
$\vec{f}$	Flux vector [Nm <sup>-2</sup> ] resp. [Wm <sup>-2</sup> ]
$I$	Current [A]
$\vec{j}$	Electric current density [Am <sup>-2</sup> ]
$\vec{j}_D$	Diffusion number flux [m <sup>-2</sup> s <sup>-1</sup> ]
$k$	Reaction rate constant [m <sup>3</sup> s <sup>-1</sup> ]
$n$	Particle density [m <sup>-3</sup> ]
$p$	Pressure [Pa]
$Q$	Collision cross section [m <sup>2</sup> ]
$Q$	Heat [W]
$q$	Source term [Nm <sup>-3</sup> ] resp. [Wm <sup>-3</sup> ]
$r$	Radial coordinate [m]
$T$	Temperature [K]
$t$	Time [s]
$u$	Drift velocity [ms <sup>-1</sup> ]
$\vec{v}$	Velocity [ms <sup>-1</sup> ]

---

\*Scientist, Institute of Space Systems, [haag@irs.uni-stuttgart.de](mailto:haag@irs.uni-stuttgart.de).

†Head of Plasma Modeling and Simulation Group, Institute of Space Systems, [fertig@irs.uni-stuttgart.de](mailto:fertig@irs.uni-stuttgart.de).

‡Prof. Dr.-Ing. habil., Universität Hamburg, President, [praesidentin@hvn.uni-hamburg.de](mailto:praesidentin@hvn.uni-hamburg.de).

$Z$	Charge number [-]
$z$	Axial coordinate [m]
$\alpha$	Degree of ionization [-]
$\alpha_{ei}$	Energy transfer coefficient [ $\text{Wm}^{-3}\text{K}$ ]
$\beta$	$1/(en_e)$ [ $\text{m}^3\text{C}^{-1}$ ]
$\chi$	Ionization energy [J]
$\lambda$	Thermal conductivity [ $\text{Wm}^{-1}\text{K}^{-1}$ ]
$\mu$	Viscosity coefficient [ $\text{kgm}^{-1}\text{s}^{-1}$ ]
$\nu$	Collision frequency [ $\text{s}^{-1}$ ]
$\Omega$	Hallparameter [-]
$\omega$	Reaction source term [ $\text{m}^{-3}\text{s}^{-1}$ ]
$\omega_c$	Cyclotron frequency [ $\text{s}^{-1}$ ]
$\omega_e$	Electron gyration frequency [ $\text{s}^{-1}$ ]
$\omega_p$	Plasma frequency [ $\text{s}^{-1}$ ]
$\Psi$	Stream function [Tm]
$\rho$	Density [ $\text{kgm}^{-3}$ ]
$\sigma$	Electrical conductivity [ $\Omega^{-1}\text{m}^{-1}$ ]
$\tau$	Mean free flight time [s]
$\tau$	Viscous stress [ $\text{Nm}^{-2}$ ]
$\varphi$	Azimuthal [-]

*Subscripts*

$A$	Anode
$AN$	Anomalous
$b$	Backward
$c$	Coil
$cell$	Cell of the computational domain
$coil$	Coil winding
$D$	Diffusion
$d$	Drift
$eff$	Effective
$e$	Electron
$ei$	Electron-Ion
$f$	Forward
$h$	Heavy particle
$i$	I-fold ionized species
$i$	Ion
$invisc$	Inviscid
$m$	Centre of mass
$r$	Radial
$t$	Thermal
$visc$	Viscous
$z$	Axial
$\varphi$	Azimuthal
$\parallel$	Parallel
$\perp$	Perpendicular

*Constants*

$e$	Elementary charge, $e = 1.60219 \cdot 10^{-19}$ C
$k$	Boltzmann constant, $k = 1.38062 \cdot 10^{-23}$ JK $^{-1}$
$m_e$	Electron mass, $m_e = 9.10956 \cdot 10^{-31}$ kg
$m_h$	Heavy particle (argon) mass, $m_h = 6.63349 \cdot 10^{-26}$ kg
$\varepsilon_0$	Permittivity of free space, $\varepsilon_0 = 8.85419 \cdot 10^{-12}$ Fm $^{-1}$
$\mu_0$	Permeability of free space, $\mu_0 = 4\pi \cdot 10^{-7}$ VsA $^{-1}\text{m}^{-1}$

## I. Introduction

STATIONARY applied field magnetoplasmadynamic (AF-MPD) thrusters in the power range 5–100 kW are promising devices for orbit control systems of large satellites, because of their high specific impulse, thrust density and efficiency.<sup>1</sup> Furthermore, AF-MPD thrusters at higher power levels appear to be excellently suited for interplanetary space missions like crewed and uncrewed Mars missions. Already in the seventies of the last century, the applied field laboratory thruster DFVLR-X16 was developed at DLR Stuttgart (formerly DFVLR). Up to now, it is one of the best devices with noble gases as propellant. The device reached a thrust of 251 mN at an effective exit velocity of 36 km/s. Efficiency of 38.8 % was achieved with an applied magnetic field of 0.6 T.<sup>2</sup>

The step to flight-qualified AF-MPD thrusters has not been taken yet. Besides the low pressure needed for experimental investigations of AF-MPD thrusters in ground test facilities, the optimization of the devices is difficult, because AF-MPD thrust depends on the distribution of interacting plasma parameters. In addition, the configuration of the applied magnetic field has a significant effect on thrust. The complex acceleration processes are not well understood yet. Therefore, efficient numerical simulation tools are needed to gain experience and to support further development.

Supported by the German Research Foundation DFG (Deutsche Forschungsgemeinschaft) a program for numerical simulations of AF-MPD thrusters is currently under development at IRS. The simulation software SAMSA (Self and applied field MPD thruster simulation algorithm) is based on a numerical code that has been developed and was qualified at IRS for the simulation of self-field MPD thrusters.<sup>3</sup> SAMSA is intended to be used to achieve a better understanding of the basic plasmaphysical processes, which lead to the acceleration of the propellant, and to optimize the thruster and electrode geometry and particularly the configuration of the applied magnetic field of an AF-MPD thruster.

In the following sections of this paper an overview on the principles of operation of AF-MPD thrusters and on the physical model as well as on the computational methods implemented in SAMSA is given. Also, numerical results are shown which have been conducted for the geometry of the laboratory AF-MPD thruster currently under development at IRS.<sup>4</sup>

## II. Physical Properties of AF-MPD Thrusters

The principle design of an AF-MPD thruster is illustrated in Fig. 1 on the following page. The thruster consists of a central cathode and a coaxial anode at the end of a nozzle-like configuration. The applied magnetic field is created by coaxial arranged coils or permanent magnets.

Acceleration and energy conversion mechanisms of AF-MPD thrusters can be derived from the generalized Ohm's law and the corresponding energy equation:<sup>5</sup>

$$\begin{aligned} \vec{j} &= \sigma \left( \vec{E} + \vec{v} \times \vec{B} \right) - \frac{\omega_e \tau_e}{|\vec{B}|} \left( \vec{j} \times \vec{B} \right) + \frac{1}{en_e} \nabla p_e \text{ and} \\ \vec{j} \cdot \vec{E} &= \frac{|\vec{j}|^2}{\sigma} + \vec{v} \left( \vec{j} \times \vec{B} \right) - \frac{1}{en_e} \vec{j} \nabla p_e . \end{aligned} \quad (1)$$

Four main acceleration mechanisms are known to be effective:<sup>1,5</sup>

1. Joule heating and thermal expansion through a nozzle.
2. Interaction of discharge current arc and self-induced azimuthal magnetic field leads to axial and radial acceleration.
3. Interaction of discharge current and applied magnetic field results in a azimuthal force that puts the plasma into rotation. The rotational energy can be partly converted to axial acceleration downstream.
4. Interaction of induced azimuthal current (Hall current) and applied magnetic field produces axial and radial Lorentz force components.

The formation of high azimuthal currents is very important to achieve high thrust. Particle collision rates have to be low to get high azimuthal currents. Therefore, the Hall parameter can be seen as the

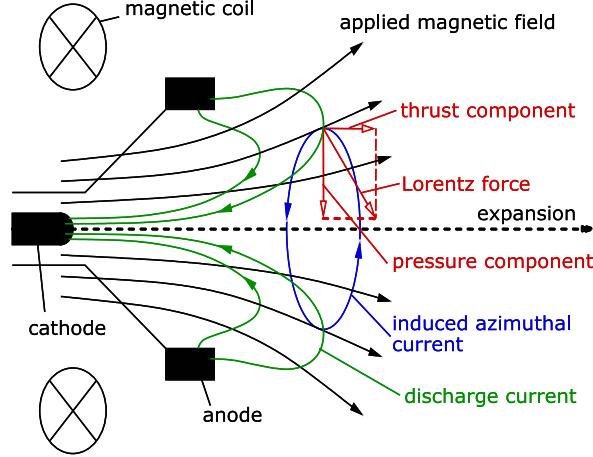


Figure 1. Principle design of an AF-MPD thruster with coaxial applied magnetic field.

characteristic parameter for AF-MPD thrusters:<sup>6</sup>

$$\Omega_e = \omega_e \tau_e = \frac{\sigma |\vec{B}|}{en_e} \propto \frac{|\vec{B}| T_e^{5/2}}{p_e} . \quad (2)$$

Equation (2) indicates that a strong magnetic field, high temperature and low pressure are necessary to gain high thrust in AF-MPD thrusters. The strong magnetic field leads to reduced electrical conductivity perpendicular to the magnetic field:

$$\sigma_{\perp} = \frac{\sigma_{\parallel}}{1 + \Omega_e^2} . \quad (3)$$

Because of the anisotropic electrical conductivity, the current stream lines are extended far outside the thruster (“magnetic nozzle effect”).<sup>6</sup> Therefore, for numerical simulations of AF-MPD thrusters the calculation domain has to be extended far downstream from the thruster. Also, this region has to be included into the calculation to allow the conversion of rotational energy into axial acceleration of the propellant mentioned above.

### III. Physical Model for the Numerical Simulations

Due to axisymmetric geometries of the plasma generator and the vacuum tank, the plasma flow inside the calculation domain is supposed to be axisymmetric as well. Hence, the conservation equations are used in a two-dimensional form with cylindrical coordinates. Considering all relevant plasma interaction mechanisms, azimuthal components have to be included into the model for electrodynamic variables, the plasma velocity and momentum. For this reason, a quasi-three dimensional approach is used with azimuthal derivatives set to zero, i.e.:

$$\text{div} \begin{pmatrix} a_r \\ a_{\varphi} \\ a_z \end{pmatrix} \equiv \frac{1}{r} \frac{\partial (ra_r)}{\partial r} + \frac{\partial a_z}{\partial z} \equiv \text{div} \begin{pmatrix} a_r \\ a_z \end{pmatrix} . \quad (4)$$

Assuming continuum flow, the argon plasma is considered as a quasineutral two-fluid plasma in thermal and chemical non-equilibrium (up to 6-fold ionized argon). No turbulence is considered due to strong viscous dissipation in the hot plasma and low pressure level in AF-MPD thrusters.

The transport coefficients of argon for viscosity of heavy particles  $\mu_h$ , thermal conductivity of heavy particles  $\lambda_h$  and electrons  $\lambda_e$  and the effective diffusion coefficients  $D_{im}$  for each of the heavy particle species, which are required by the conservation equations, are calculated according to Heiermann and Auweter-Kurtz.<sup>3,7</sup>

### III.A. Anomalous Diffusion

Early numerical calculations performed with SAMSA showed perturbations in the current distribution of the arc discharge.<sup>8</sup> In areas in which these perturbations occurred the electron particle density decreased. These perturbations lead to instabilities in the calculations and limited the time step and convergence. At values of the applied magnetic field above 0.1 T the electron particle density decreased even more and the calculations did not converge any more.

Because of the low density level, respectively pressure level, in AF-MPD thrusters the classical electrical conductivity seems not to describe the transport processes in the plasma adequately. One effect which can occur is anomalous diffusion. For the electrical conductivity  $\sigma$  anomalous diffusion has been included to investigate the impact on the numerical simulations. The computational effort for the calculation of the anomalous diffusion has to be low because of the overall limitation of calculating capacity. A frugal method with regard to the computational costs has been presented by Choueiri based on interpolating polynomials.<sup>9</sup>

The effective electrical conductivity is now given by

$$\sigma = \sigma_{eff} = \frac{3}{4} \frac{e^2 n_e}{m_e \left( \sum_{i=0}^6 (\nu_{ei}) + \nu_{AN,e} \right)}, \quad (5)$$

where  $\nu_{ei}$  is the collision frequency between electrons and  $i$ -fold ionized argon

$$\nu_{ei} = n_i Q_{ei} \sqrt{\frac{8kT_e}{\pi m_e}} \quad (6)$$

and  $Q_{ei}$  is the Gvosdover collision cross section for collisions of electrons and argon ions.<sup>3</sup>

According to Choueiri, similar to the association of classical conductivity with the coulomb collision frequency  $\nu_{ei}$ , the anomalous conductivity is associated with the effective momentum exchange rate or frequency  $\nu_{AN,e}$  between electrons and the turbulent fluctuating fields caused by cross-field current-driven instabilities.<sup>9</sup> For the numerical simulations this effective frequency  $\nu_{AN,e}$  is computed through an interpolating polynomial:<sup>9</sup>

$$\begin{aligned} \nu_{AN,e} = & \sum_{i=0}^6 (\nu_{ei}) \left[ 0.192 + 3.33 \cdot 10^{-2} \Omega_e + 0.212 \Omega_e^2 + 8.27 \cdot 10^{-5} \Omega_e^3 \right. \\ & \left. + \frac{T_h}{T_e} \left( 1.23 \cdot 10^{-3} - 1.58 \cdot 10^{-2} \Omega_e - 7.89 \cdot 10^{-3} \Omega_e^2 \right) \right]. \end{aligned} \quad (7)$$

The ions are heated by the turbulent fluctuations through

$$Q_{AN,i} = \frac{3}{2} k T_h \nu_{AN,i}, \quad (8)$$

which is taken into account in the conservation equation of heavy particles energy Eq. (20) as a source term. The collision heating rate  $\nu_{AN,i}$  is again computed by an interpolating polynomial:<sup>9</sup>

$$\begin{aligned} \nu_{AN,i} = & \sum_{i=0}^6 (\nu_{ei}) \left[ 5.36 \cdot 10^{-5} + 1.29 \cdot 10^{-5} \Omega_e + 6.03 \cdot 10^{-6} \Omega_e^2 + 9.44 \cdot 10^{-8} \Omega_e^3 \right. \\ & \left. + \frac{T_h}{T_e} \left( -7.55 \cdot 10^{-7} - 5.41 \cdot 10^{-6} \Omega_e - 3.93 \cdot 10^{-6} \Omega_e^2 \right) \right]. \end{aligned} \quad (9)$$

According to Choueiri<sup>9</sup> the ratio of electron drift velocity to thermal velocity of ions must exceed a threshold for the anomalous transport to be operative. The ratio is calculated by

$$\frac{u_{d,e}}{v_{t,i}} = \frac{|\vec{j}|}{en_e} \sqrt{\frac{m_h}{2kT_h}}. \quad (10)$$

If  $u_{d,e}/v_{t,i} < 1.5$  both  $\nu_{AN,e}$  and  $\nu_{AN,i}$  are set to zero and there is only classical transport. Furthermore, the electron Hall parameter  $\Omega_e$  should not exceed 10 and the ratio of plasma frequency to cyclotron frequency

$$\frac{\omega_{p,e}}{\omega_{c,e}} = \frac{\sqrt{\frac{n_e m_e}{\epsilon_0}}}{|\vec{B}|} \quad (11)$$

should be greater 10.

### III.B. Conservation of Mass

Conservation of mass is expressed as balance of particle densities for each heavy particle species:

$$\frac{\partial n_i}{\partial t} = -\text{div}(n_i \vec{v}) - \text{div} \vec{j}_{D,i} + \omega_i . \quad (12)$$

Diffusion fluxes  $\vec{j}_{D,i}$  are computed with Fick's law for multicomponent mixtures.<sup>3,7</sup> A conservation equation for electron particle density is not needed because of the assumption of a quasineutral plasma.

The chemical source term  $\omega_i$  includes electron impact ionization and three-body recombination:

$$\begin{aligned} \omega_0 &= -n_0 n_e k_{f,1} + n_1 n_e^2 k_{b,1} , \\ \omega_i &= +n_{i-1} n_e k_{f,i} - n_i n_e^2 k_{b,i} - n_i n_e k_{f,i+1} + n_{i+1} n_e^2 k_{b,i+1} , \\ \omega_6 &= +n_5 n_e k_{f,6} - n_6 n_e^2 k_{b,6} . \end{aligned} \quad (13)$$

The forward reaction rate constants  $k_{f,i}$  and the backward reaction rate constants  $k_{b,i}$  are calculated according to Heiermann and Auweter-Kurtz.<sup>3,7</sup>

### III.C. Conservation of Momentum

The conservation equation for radial momentum is given by

$$\begin{aligned} \frac{\partial(\rho v_r)}{\partial t} &= -\text{div} \vec{f}_{invisc}^{\rho v_r} - \text{div} \vec{f}_{visc}^{\rho v_r} + q^{\rho v_r}, \text{ where} \\ \vec{f}_{invisc}^{\rho v_r} &= \begin{pmatrix} \rho v_r^2 + p_h + p_e \\ \rho v_r v_z \end{pmatrix} \text{ is the inviscid flux,} \\ \vec{f}_{visc}^{\rho v_r} &= \begin{pmatrix} -\tau_{rr} \\ -\tau_{rz} \end{pmatrix} \text{ is the viscous flux and} \\ q^{\rho v_r} &= \frac{\rho v_\varphi^2 + p_h + p_e - \tau_{\varphi\varphi}}{r} + (j_\varphi B_z - j_z B_\varphi) \text{ is the source term.} \end{aligned} \quad (14)$$

The first term of the source term arises from using cylindrical coordinates.<sup>10</sup> The second term describes the effect of electromagnetic interaction.

The conservation equation of azimuthal momentum is given by

$$\begin{aligned} \frac{\partial(\rho v_\varphi)}{\partial t} &= -\text{div} \vec{f}_{invisc}^{\rho v_\varphi} - \text{div} \vec{f}_{visc}^{\rho v_\varphi} + q^{\rho v_\varphi}, \text{ where} \\ \vec{f}_{invisc}^{\rho v_\varphi} &= \begin{pmatrix} \rho v_r v_\varphi \\ \rho v_\varphi v_z \end{pmatrix} \text{ is the inviscid flux,} \\ \vec{f}_{visc}^{\rho v_\varphi} &= \begin{pmatrix} -\tau_{r\varphi} \\ -\tau_{\varphi z} \end{pmatrix} \text{ is the viscous flux and} \\ q^{\rho v_\varphi} &= \frac{\tau_{r\varphi} - \rho v_r v_\varphi}{r} + (j_z B_r - j_r B_z) \text{ is the source term.} \end{aligned} \quad (15)$$

The conservation equation of axial momentum is given by

$$\begin{aligned} \frac{\partial(\rho v_z)}{\partial t} &= -\text{div} \vec{f}_{invisc}^{\rho v_z} - \text{div} \vec{f}_{visc}^{\rho v_z} + q^{\rho v_z}, \text{ where} \\ \vec{f}_{invisc}^{\rho v_z} &= \begin{pmatrix} \rho v_r v_z \\ \rho v_z^2 + p_h + p_e \end{pmatrix} \text{ is the inviscid flux,} \\ \vec{f}_{visc}^{\rho v_z} &= \begin{pmatrix} -\tau_{rz} \\ -\tau_{zz} \end{pmatrix} \text{ is the viscous flux and} \\ q^{\rho v_z} &= (j_r B_\varphi - j_\varphi B_r) \text{ is the source term.} \end{aligned} \quad (16)$$

The viscous stresses are given by

$$\begin{aligned} \tau_{rr} &= \frac{2}{3}\mu_h \left( 2\frac{\partial v_r}{\partial r} - \frac{v_r}{r} - \frac{\partial v_z}{\partial z} \right), & \tau_{\varphi\varphi} &= \frac{2}{3}\mu_h \left( 2\frac{v_r}{r} - \frac{\partial v_r}{\partial r} - \frac{\partial v_z}{\partial z} \right), & \tau_{zz} &= \frac{2}{3}\mu_h \left( 2\frac{\partial v_z}{\partial z} - \frac{v_r}{r} - \frac{\partial v_r}{\partial r} \right), \\ \tau_{r\varphi} &= \tau_{\varphi r} = \mu_h \left( \frac{\partial v_\varphi}{\partial r} - \frac{v_\varphi}{r} \right), & \tau_{rz} &= \tau_{zr} = \mu_h \left( \frac{\partial v_z}{\partial r} - \frac{\partial v_r}{\partial z} \right) & \text{and} & \tau_{\varphi z} = \tau_{z\varphi} = \mu_h \frac{\partial v_\varphi}{\partial z}. \end{aligned} \quad (17)$$

### III.D. Conservation of Energy

With the equation of state for heavy particle pressure

$$p_h = n_h k T_h, \quad (18)$$

heavy particle energy  $e_h$ , which is composed of translatory and kinetic energy, is defined as:

$$e_h = \frac{3}{2}n_h k T_h + \frac{1}{2}\rho |\vec{v}|^2. \quad (19)$$

The conservation equation for heavy particle energy is given by:

$$\begin{aligned} \frac{\partial e_h}{\partial t} &= -\text{div} \vec{f}_{invisc}^{e_h} - \text{div} \vec{f}_{visc}^{e_h} + q^{e_h}, \quad \text{where} \\ \vec{f}_{invisc}^{e_h} &= \left( (e_h + p_h + p_e) \begin{pmatrix} v_r \\ v_z \end{pmatrix} \right) \text{ is the inviscid flux,} \\ \vec{f}_{visc}^{e_h} &= \begin{pmatrix} -\tau_{rr}v_r - \tau_{r\varphi}v_\varphi - \tau_{rz}v_z - \lambda_h \frac{\partial T_h}{\partial r} \\ -\tau_{rz}v_r - \tau_{\varphi z}v_\varphi - \tau_{zz}v_z - \lambda_h \frac{\partial T_h}{\partial r} \end{pmatrix} \text{ is the viscous flux and} \\ q^{e_h} &= p_e \text{div} \vec{v} + \vec{v} \cdot (\vec{j} \times \vec{B}) + \sum_{i=0}^6 n_i n_e \alpha_{ei} (T_e - T_h) + \frac{3}{2}n_h k T_h \nu_{AN,i} \text{ is the source term.} \end{aligned} \quad (20)$$

The flux vector  $\vec{f}_{visc}^{e_h}$  includes fluxes created by viscous forces and heat conduction of heavy particles. In the source term  $q^{e_h}$  the first term arises because the electron pressure is included in the inviscid flux  $\vec{f}_{invisc}^{e_h}$ . The second term describes the power due to the Lorentz force, the third term describes the energy transfer between electrons and heavy particles and the last term models ion heating by turbulent fluctuations.

With electron pressure defined as

$$p_e = n_e k T_e \quad (21)$$

and electron energy

$$e_e = \frac{3}{2}n_e k T_e, \quad (22)$$

the conservation equation of electron energy is given by

$$\begin{aligned} \frac{\partial e_e}{\partial t} &= -\text{div} (e_e \vec{v}_e) - p_e \text{div} \vec{v}_e - \text{div} \left( \frac{3}{2}k T_e \vec{j}_{D,e} \right) + \text{div} (\lambda_e \nabla T_e) \\ &+ \sum_{i=0}^6 n_i n_e \alpha_{ei} (T_h - T_e) + \frac{|\vec{j}|^2}{\sigma} - \sum_{i=0}^5 \omega_{i+1} \chi_{i \rightarrow i+1}. \end{aligned} \quad (23)$$

The terms on the right hand side of Eq. (23) describe convective transport caused by electron velocity  $\vec{v}_e$ , deformation of an electron fluid element due to electron pressure, transport caused by diffusion flux  $\vec{j}_{D,e}$ , electron heat conduction, energy transfer between electrons and heavy particles, Ohmic heating and energy balance due to ionization.

By defining the current density

$$\vec{j} = en_e (\vec{v} - \vec{v}_e) \quad (24)$$

and utilizing the assumption of a quasineutral plasma, Eq. (23) can be transformed to

$$\begin{aligned} \frac{\partial e_e}{\partial t} &= -\text{div} (e_e \vec{v}) - p_e \text{div} \vec{v} + \frac{5}{2} \frac{k}{e} \vec{j} \cdot \nabla T_e - \frac{1}{en_e} \vec{j} \cdot \nabla p_e - \text{div} \left( \frac{3}{2}k T_e \sum_{i=1}^6 Z_i \vec{j}_{D,i} \right) + \text{div} (\lambda_e \nabla T_e) \\ &+ \sum_{i=0}^6 n_i n_e \alpha_{ei} (T_h - T_e) + \frac{|\vec{j}|^2}{\sigma} - \sum_{i=0}^5 \omega_{i+1} \chi_{i \rightarrow i+1}. \end{aligned} \quad (25)$$

### III.E. Conservation of the Magnetic Field

Using Ohm's law for plasmas (Eq. (1)) and the Maxwell Equations,<sup>11,12</sup> conservation equations for the axial, radial and azimuthal components of the magnetic field can be achieved. In self-field MPD thrusters only the azimuthal component of these conservation equations is necessary to describe the arc discharge between cathode and anode and the induced magnetic field.<sup>3,7</sup>

In AF-MPD thrusters the axial and radial components are additionally needed to include the influence of the applied magnetic field and induced azimuthal current density. These influences are described employing the vector potential formulation:<sup>12</sup>

$$\vec{B}\Big|_{r,z} = \begin{pmatrix} B_r \\ 0 \\ B_z \end{pmatrix} = \text{rot} \begin{pmatrix} 0 \\ A \\ 0 \end{pmatrix}. \quad (26)$$

By using the vector potential formulation, the computation of boundary values influenced by the magnetic field, which is created by solenoidal coil currents, and the induced azimuthal currents can be managed, as will be shown in section IV. The zero divergence constraint is also satisfied for the quasi-three dimensional approach ( $\partial/\partial\varphi = 0$ ):

$$\text{div} \begin{pmatrix} 0 \\ B_\varphi \\ 0 \end{pmatrix} + \text{div} \left( \text{rot} \begin{pmatrix} 0 \\ A \\ 0 \end{pmatrix} \right) = 0. \quad (27)$$

The conservation equation for the azimuthal component of the magnetic field is given by

$$\frac{\partial B_\varphi}{\partial t} = -\text{rot} \left( -\vec{v} \times \vec{B} + \frac{\text{rot} \vec{B}\Big|_\varphi}{\mu_0 \sigma} + \frac{\beta}{\mu_0} \text{rot} \vec{B} \times \vec{B} - \beta \nabla p_e \right) \Big|_\varphi, \quad \text{where } \beta = \frac{1}{en_e}. \quad (28)$$

The first term in the rot-term on the right hand side describes the convective transport of the magnetic field. The following terms describe the variation of the magnetic field, which is caused by electric current, Hall current and the diffusion flux by electron pressure. In Eq. (28) the magnetic flux density  $B_\varphi$  can be substituted by the stream function

$$\Psi = r B_\varphi. \quad (29)$$

For steady state conditions, the electric current is constant between two contour lines of the stream function  $\Psi$ . The conservation equation for the axial and radial magnetic field in vector potential formulation is given by

$$\frac{\partial A}{\partial t} = \frac{1}{\mu_0 \sigma} \text{div} (\nabla A) + \vec{v} \times \vec{B} - \beta (\vec{j} \times \vec{B}) - \frac{A}{\mu_0 \sigma r^2}. \quad (30)$$

The three components of the current density are computed by

$$\begin{aligned} j_r &= -\frac{1}{\mu_0 r} \frac{\partial \Psi}{\partial z}, \\ j_\varphi &= \sigma (v_z B_r - v_r B_z) - \beta \sigma (j_z B_r - j_r B_z) \quad \text{and} \\ j_z &= \frac{1}{\mu_0 r} \frac{\partial \Psi}{\partial r}. \end{aligned} \quad (31)$$

## IV. Computational Methods

By using unstructured meshes for the discretization of the computational domain, SAMSA is capable of simulating the plasma flow inside different self- and applied-field thrusters including the downstream region outside of the thrusters without much effort. Only the description of the geometric boundaries of these thrusters is necessary. The unstructured meshes used consist of triangles produced by an advancing front algorithm.<sup>13,14</sup> Based on these primary triangles, so-called dual cells are constructed. The corners of these dual cells are in the centers of mass of the primary triangles.<sup>3,7</sup> On cylindrical coordinates the dual cells represent toroidal control volumes which contain the average values of variables computed during the

numerical simulations. By using adaptation techniques, computational time can be reduced and accuracy can be increased.

The hyperbolic part of the conservation equations has to be solved by an adequate upwind scheme. In AF-MPD thrusters with three-dimensional magnetic fields the physical eigenvalues correspond to one entropy wave, two Alfvén waves and four magnetosonic waves (two slow and two fast). The choice of a numerical scheme is based on its accuracy and robustness. For example, Roe-type solvers are very accurate but not particularly robust for MPD calculations.<sup>15</sup> In addition, Roe solvers are computationally very expensive. The approach used here for the computation of the hyperbolic part of the conservation equations is a HLLE scheme.<sup>15–17</sup> The full Riemann solution at the cell faces is approximated by a single intermediate state bounded by two waves. Their wave speeds are density-averaged numerical approximations to the physical minimum and maximum wave speeds, which are the fast magnetosonic waves, for that particular Riemann problem. The intermediate state can be calculated by the condition of conservation.<sup>18</sup>

To achieve second order accuracy in space, all variables needed to compute the inviscid fluxes through the cell faces of the dual cells have to be linearly reconstructed. Within the scope of this work a second-order Weighted Essentially Non-Oscillatory (WENO) scheme is used.<sup>3,19</sup>

Independent of the discretization method used for the hyperbolic part of the conservation equations, the parabolic fluxes are computed by a central scheme. On unstructured grids simple central differences expressions used on structured grids can not be applied. Therefore, according to Heiermann the fluxes are evaluated on each triangle with Cramers rule to achieve a quasi-central scheme.<sup>3</sup> All other differentials needed for the calculations are computed by the least-square method.

To achieve a steady-state solution, time integration is done by explicit, randomized local time steps.<sup>3</sup>

#### IV.A. Boundary Conditions

On the inlet boundary the mass flow rate and temperature are specified and kept constant by a numerical flow controller.<sup>3</sup> On solid walls the no-slip boundary condition is implemented. Flow velocity is set to zero, heavy particle temperature is set to a specified wall temperature and electrons are assumed to behave adiabatic. On the outlet boundary subsonic or supersonic outflow conditions are used depending on the local Mach number. It is also possible to simulate recirculation of remaining gas in a vacuum tank. If the plasma velocity vector points inwards at the outlet boundary, predefined ambient conditions are used.

The electric field is assumed to be perpendicular to the electrode surfaces. On boundary cells  $\omega$  upstream from the electrodes the value of the stream function  $\Psi$  is defined by Ampères law with the discharge current  $I_A$ :

$$\Psi_\omega = \frac{\mu_0 I_A}{2\pi} . \quad (32)$$

On boundary cells downstream from the electrodes the stream function is zero.

According to Jackson<sup>12</sup> and Heiermann<sup>20</sup> the vector potential  $A$  at cell  $\omega$  caused by the solenoidal coil current  $I_c$  and by induced azimuthal current density  $j_\varphi$  is given by

$$A_\omega = I_c \frac{\mu_0}{2\pi} \underbrace{\sum_{c=1}^{N_{coil}} \left[ \sqrt{\frac{r_c}{r_{m,\omega}}} G(k) \right]}_{\text{Preprocessing}} + \frac{\mu_0}{2\pi} \sum_{i=1, i \neq \omega}^{N_{cell}} \underbrace{\left[ \sqrt{\frac{r_c}{r_{m,\omega}}} \Delta A_i G(k) j_{\varphi,i} \right]}_{\text{Preprocessing}} \quad (33)$$

with the definitions

$$G(k) = \frac{(2 - k^2) K(k) - 2E(k)}{k} , \quad (34)$$

$$k = \sqrt{\frac{4r_c r_{m,\omega}}{(r_c + r_{m,\omega})^2 + (z_{m,\omega} - z_c)^2}}$$

and the elliptic integrals

$$E(k) = \int_0^{\frac{\pi}{2}} \sqrt{1 - k^2 \sin^2 \varphi} d\varphi , \quad (35)$$

$$K(k) = \int_0^{\frac{\pi}{2}} \frac{d\varphi}{\sqrt{1 - k^2 \sin^2 \varphi}}.$$

These elliptic integrals are solved by Gauß–Legendre integration.<sup>20, 21</sup> In Eq. (33) and (34) the solenoidal coil is modelled as an array of ring-shaped windings. The coordinates  $r_c$  and  $z_c$  of each winding can be specified separately, so complicated coil configurations can be handled. The computation of the elliptic integrals is computationally very expensive. Therefore, as indicated in Eq. (33), the calculation of the geometric factors influenced by the elliptic integrals is done once before a numerical simulation is started for a given thruster and coil geometry and once after every adaptation of the mesh.

## V. Numerical Results

Numerical simulations of an AF–MPD thruster have been accomplished with SAMSA for the thruster geometry aligned with the laboratory model currently under development at IRS.<sup>4</sup> Within these calculations the full system of conservation equations for an argon plasma flow under thermal and chemical non–equilibrium has been used, which is described in Sec. III. The calculations have been made with anomalous diffusion included in the physical model. These numerical results were compared to the outcome of calculations made without the inclusion of anomalous diffusion. The DFVLR–X16 thruster geometry, which is mostly identical to the laboratory thruster of IRS, has been used for the simulations without anomalous diffusion.<sup>8</sup> Both thrusters have an outer anode diameter of  $\varnothing_A = 40$  mm. The propellant is fed through a hollow cathode with the mass flow  $\dot{m}_C$  and through an annular gap near the anode with the mass flow  $\dot{m}_A$ .

The coil geometry assumed for the DFVLR–X16 thruster calculation<sup>8</sup> consisted of 15 layers of windings and 10 windings in each layer. The calculation for the IRS laboratory model has been made for a magnetic coil consisting of 16 layers of windings with 10 windings in each layer. Compared to the calculations for the X16 thruster, the axial distance between the anode tip and the front side of the magnetic coil assumed for the IRS laboratory model is slightly larger. At the same coil current  $I_c$  this results in lower applied magnetic field strength at the reference point on the centerline in front of the cathode. The axial distance between the magnetic coil and anode of the IRS laboratory model is variable. One goal of the numerical simulations for the laboratory model is to find the optimum distance for maximum thrust in the future.

The simulations neglecting anomalous diffusion are not stable, if the applied magnetic field strength exceeds  $B = 0.1$  T. Only by limiting the factor  $\beta = 1/(en_e)$  in the conservation equation for the azimuthal magnetic field Eq. (28) to 0.05 the simulation converged. Therefore, the calculations shown in the following have been made for an applied magnetic field of  $B = 0.1$  T to compare the influence of anomalous diffusion on the plasma flow. As mentioned in Sec. III.A on page 5, the implemented anomalous diffusion model requires that the ratio of electron drift velocity to thermal speed of the ions exceeds a threshold of 1.5 in order that the anomalous diffusion is operative. Furthermore, the Hallparameter  $\Omega_e$  should not exceed 10. Both conditions could not be fulfilled in the complete calculation domain, because of the low ambient pressure necessary for AF–MPD thrusters to be working. The electron particle density in the area downstream of the thruster is too low to allow for a threshold value greater than 1.5 and a Hallparameter lower than 10. The area downstream of the thruster can not be neglected, because the main part of propellant acceleration happens in this domain. If a distinction is made for the calculation of the electrical conductivity, depending on the threshold, a discontinuity arises in the distribution of the electrical conductivity, which prevented convergence. Neglecting the threshold allowed convergence if simultaneously the ion heating term in the conservation equation of heavy particle energy was also neglected and the Hallparameter  $\Omega_e$  for the calculation of the effective frequency  $\nu_{AN,e}$  in Eq. (7) was limited to 5.0. Including the ion heating term lead to an unlimited temperature rise in the area downstream of the thruster. The limitation of  $\beta = 1/(en_e)$  could be eased to 5.0 in Eq. (28) by including anomalous diffusion.

Table 1 on the next page outlines the operating parameters of the two thrusters which have been used for the calculations shown in the following. The left columns of Fig. 2 on page 14 and Fig. 3 on page 15 show the results of the calculations without anomalous diffusion. The right columns summarize the results for the calculations with anomalous diffusion and neglecting the ion heating term. At a coil current of  $I_c = 100$  A the resulting applied magnetic field on the centerline at the cathode tip became  $B = 0.1$  T for the DFVLR–X16 thruster and  $B = 0.084$  T for the IRS laboratory thruster. For the results shown in the following the discharge current was  $I_A = 80$  A, the cathode gas flow  $\dot{m}_C = 5$  mg/s and the anode gas flow  $\dot{m}_A = 2$  mg/s in both thrusters.

Table 1. Operating parameters for numerical simulations; results shown in Fig. 2 on page 14 and Fig. 3 on page 15.

	DFVLR–X16 geometry: (no anomalous diffusion included) <sup>8</sup>	IRS laboratory thruster: (anomalous diffusion included)
Outer diameter of anode	$\varnothing_A = 40$ mm	$\varnothing_A = 40$ mm
Cathode mass flow rate	$\dot{m}_C = 5$ mg/s	$\dot{m}_C = 5$ mg/s
Anode mass flow rate	$\dot{m}_A = 2$ mg/s	$\dot{m}_A = 2$ mg/s
Discharge current	$I_A = 80$ A	$I_A = 80$ A
Coil geometry	15 layers, each with 10 windings	16 layers, each with 10 windings
Coil current	$I_c = 100$ A	$I_c = 100$ A
Applied magnetic field	$B = 0.1$ T	$B = 0.084$ T

Figure 2(a) on page 14 shows the degree of ionization  $\alpha = n_e/n_h$  in the calculation domain for the simulation without anomalous diffusion. In Fig. 2(b) the degree of ionization  $\alpha$  is shown for anomalous diffusion without the ion heating term included. The distribution of electron temperature  $T_e$  is shown in Fig. 2(c) and 2(d). Figures 2(e) and 2(f) show the corresponding distribution of heavy particle temperature  $T_h$ . The non-equilibrium between electrons and heavy particles is clearly noticeable in both cases. As a result of the low particle density, the collision frequencies and the energy exchange between the particles are low. Because of their low mass and high mobility, the electrons are assumed to carry the electric current in the plasma. Therefore, the electron temperature is increased by Ohmic heating. Only a small part of the energy is transferred to the heavy particles. The electron and heavy particle temperatures are noticeable higher in the calculations including anomalous diffusion. This leads to significantly higher degrees of ionization.

Figures 3(a) and 3(b) on page 15 show the distribution of heavy particle density  $\log_{10} \rho$ . For the calculations without anomalous diffusion at an increasing applied magnetic field an area of low density appears inside the thruster, and the constriction of the plasma flow in front of the anode gets stronger. This limits the convergence rate of SAMSA because of time step restrictions caused by the viscous flux terms. For the calculations including anomalous diffusion without the ion heating term the depletion of density inside the thruster is weaker and also the time for reaching convergence is shorter.

In Fig. 3(c) and 3(d) on page 15 the current distribution  $\Psi$  is given. The current stream lines are carried far more downstream in the anomalous diffusion case. The contour lines of the current distribution show perturbations in front of the electrodes which rise with increasing strength of the applied magnetic field. A reduction of the perturbations in the anomalous diffusion case downstream of the thruster is possible by further refinement of the mesh which is comparatively coarse for this calculation. Especially for the thruster geometry shown here these perturbations become obvious inside the thruster also. The perturbations inside the thruster increase as the particle density decreases with stronger applied magnetic fields. This can be traced back to the Hall term of the azimuthal induction equation Eq. (28), which is inversely proportional to electron density. With increasing values of the applied magnetic field this leads to instabilities in the numerical calculations for the model without anomalous diffusion. The simulations including anomalous diffusion show a more stable behaviour.

Figures 3(e) and 3(f) on page 15 show the axial velocity distributions. The axial velocity for the simulation including anomalous diffusion shows a higher velocity maximum downstream of the thruster exit plane. But compared to the experimentally gained values for the DFVLR–X16 thruster,<sup>2</sup> the calculated axial velocity remains far too low. Although the limitation of  $\beta = 1/(en_e)$  has been eased by two magnitudes to 5.0 compared to the calculation without anomalous diffusion, the acceleration mechanism caused by the Hall term in the conservation equation of the azimuthal magnetic field Eq. (28) can not work effectively, if a limitation occurs.

## VI. Conclusion

The numerical simulation program SAMSA as described in this paper allows simulations of argon plasma flows in AF–MPD thrusters. Parametric analyses of electrode configuration, nozzle geometry and configuration of the solenoidal coils are possible. These analyses are eased by using a finite volume scheme on

unstructured meshes, which allows for fast customization to various, complicated thruster geometries. In addition, the configuration of the solenoidal coil can be changed with minimum effort.

The calculations for the investigated AF-MPD thruster geometries using the physical model including anomalous diffusion perform more stable than the calculations without anomalous diffusion. The results show higher temperature maximums and higher degrees of ionization for the calculations with anomalous diffusion. Also, the axial velocity is higher. However, the calculated velocities are far lower than expected in comparison to reference values. To allow for convergence of the calculation, the anomalous diffusion model and the discretization used for the conservation equation of the azimuthal magnetic field demand a lower limit of the electron particle density, which can not be fulfilled in the whole calculation domain. Consequently, the acceleration mechanisms of AF-MPD thrusters are not modelled correctly by SAMSA at the moment and further improvements are necessary.

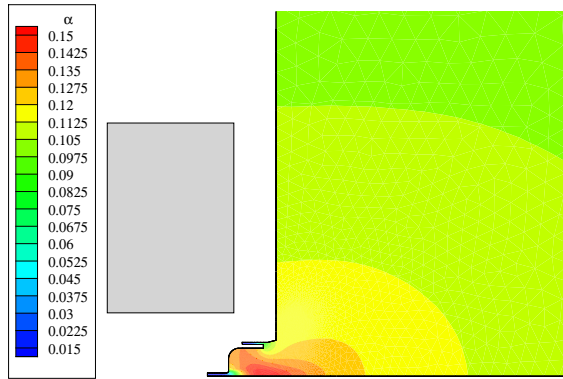
## Acknowledgments

The authors wish to thank the German Research Foundation DFG (Deutsche Forschungsgemeinschaft) for the financial support through the project “Numerische Simulation zur Auslegung eines magnetoplasma-dynamischen Triebwerks mit überlagertem koaxialem Magnetfeld” (Au 88/25-2).

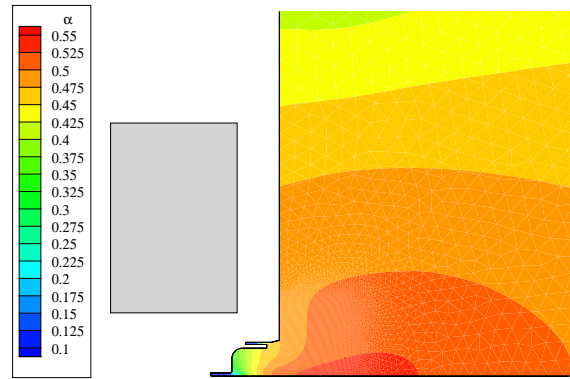
## References

- <sup>1</sup>Kurtz, H., Auweter-Kurtz, M., and Heiermann, J., “Magnetoplasma-dynamic Thrusters with Coaxial Applied Field,” *Propulsion 2000, IRS-02-P13, Final Version, Institute of Space Systems, Universität Stuttgart, Stuttgart, Germany*, 2002.
- <sup>2</sup>Krülle, G., Auweter-Kurtz, M., and Sasoh, A., “Technology and Application Aspects of Applied Field Magnetoplasma-dynamic Propulsion,” *Journal of Propulsion and Power, Vol. 14, No. 5*, 1998.
- <sup>3</sup>Heiermann, J., “A Finite Volume Method for the Solution of Magnetoplasma-dynamic Conservation Equations,” *Doctoral Thesis, Institut für Raumfahrtsysteme, Universität Stuttgart, Stuttgart, Germany*, 2002.
- <sup>4</sup>Haag, D., Auweter-Kurtz, M., Fertig, M., Herdrich, G., Kurtz, H., and Winter, M., “Experimental Investigations of Magnetoplasma-dynamic Thrusters with Coaxial Applied Magnetic Field,” *IEPC-2007-141, 30th International Electric Propulsion Conference, Florence, Italy*, 2007.
- <sup>5</sup>Krülle, G., “On the Dynamics of the Axisymmetric Magnetoplasma-dynamic Accelerator (MPD Thruster) with Applied Magnetic Field,” *Ph. D. Thesis, Technical University of Munich, DLR FB-74-56, DFVLR, Munich, Germany*, 2002.
- <sup>6</sup>Auweter-Kurtz, M., “Lichtbogenantriebe für Weltraumaufgaben,” *B.G. Teubner-Verlag, Stuttgart, Germany*, 1992.
- <sup>7</sup>Heiermann, J. and Auweter-Kurtz, M., “Numerical and Experimental Investigation of the Current Distribution in Self-Field MPD Thrusters,” *AIAA Paper 2001-3498*, 2001.
- <sup>8</sup>Haag, D., Auweter-Kurtz, M., Fertig, M., and Kurtz, H., “Development of an Applied Field Magnetoplasma-dynamic Thruster Design Supported by Numerical Simulations at IRS,” *29th International Electric Propulsion Conference, Princeton*, 2005.
- <sup>9</sup>Choueiri, E. Y., “Anomalous resistivity and heating in current-driven plasma thrusters,” *Physics of Plasmas, Vol. 6, No. 5*, 1999.
- <sup>10</sup>Trostel, R., “Vektor- und Tensoranalysis,” *Vieweg-Verlag, Wiesbaden, Germany*, 1997.
- <sup>11</sup>Cap, F., “Lehrbuch der Plasmaphysik und Magnetohydrodynamik,” *Springer-Verlag, Wien, Austria*, 1994.
- <sup>12</sup>Jackson, J. D., “Classical Electrodynamics,” *2nd ed., John Wiley and Sons*, 1975.
- <sup>13</sup>Boie, C., Auweter-Kurtz, M., Kaeppler, H. J., and Sleziona, P. C., “Numerical Simulation of MPD Thrusters on Adaptive Unstructured Mesh,” *Computational Fluid Dynamics 94, edited by S. Wagner, E. A. Hirschel, J. Periaux and R. Piva, John Wiley and Sons*, 1994.
- <sup>14</sup>Boie, C., “Numerische Simulation magnetoplasma-dynamischer Eigenfeldtriebwerke mit hochauflösenden adaptiven Verfahren,” *Doctoral Thesis, Institut für Raumfahrtsysteme, Fakultät Luft- und Raumfahrttechnik, Universität Stuttgart, Stuttgart*, 1999.
- <sup>15</sup>Linde, T. J., “A Three-Dimensional Adaptive Multifluid MHD Model of the Heliosphere,” *Ph. D. Dissertation, University of Michigan*, 1998.
- <sup>16</sup>Harten, A., Lax, P. D., and van Leer, B., “On Upstream Differencing and Godunov-Type Schemes for Hyperbolic Conservation Laws,” *SIAM Review, Vol. 25, No. 1*, 1983.
- <sup>17</sup>Einfeldt, B., “On Godunov-Type Methods for Gas Dynamics,” *SIAM Journal on Numerical Analysis, Vol. 25, No. 2*, 1988.
- <sup>18</sup>LeVeque, R. J., “Nonlinear Conservation Laws and Finite Volume Methods for Astrophysical Fluid Flow,” *Computational Methods for Astrophysical Fluid Flow, edited by O. Steiner and A. Gautschy, Springer-Verlag*, 1998.
- <sup>19</sup>Friedrich, O., “Weighted Essentially Non-Oscillatory Schemes for the Interpolation of Mean Values on Unstructured Grids,” *Journal of Computational Physics, Vol. 144, No.1*, 1998.
- <sup>20</sup>Heiermann, J., Auweter-Kurtz, M., Lenzner, S., and Sleziona, P. C., “Erstellung eines elektrodynamischen Programmmoduls zur Modellierung der Plasmaströmung in einem HF-Generator mit Hilfe der Methode der Finiten Differenzen auf einem strukturiert krummlinigen Netz,” *Diploma Thesis, IRS-97-S25, Institut für Raumfahrtsysteme, Universität Stuttgart, 1997; DGLR-JT98-196, DGLR Jahrbuch, ISSN 0070-4083, pp. 923-928*, 1998.

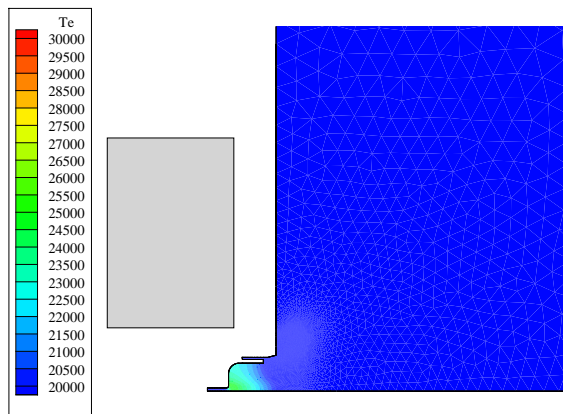
<sup>21</sup>Banerjee, P. K., "The Boundary Element Methods in Engineering," *McGraw-Hill*, 1994.



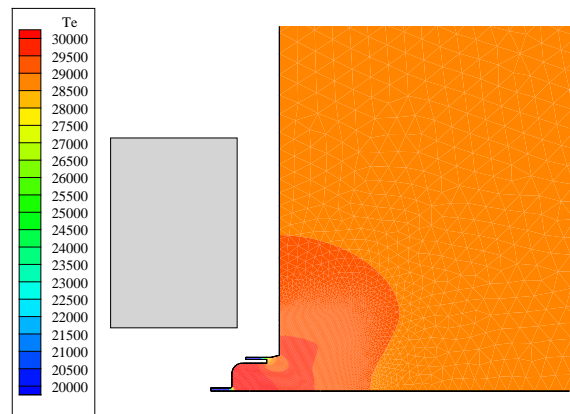
(a) Degree of ionization  $\alpha$ , no anomalous diffusion included.



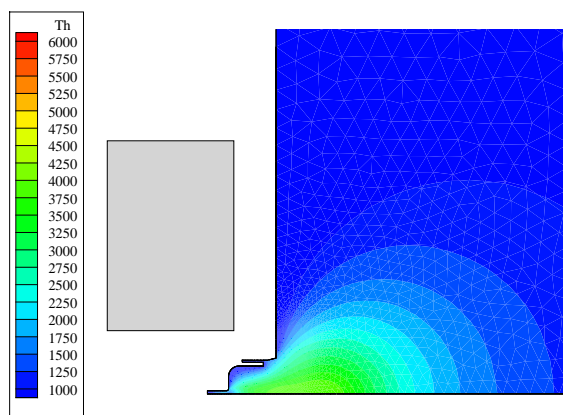
(b) Degree of ionization  $\alpha$ , anomalous diffusion included.



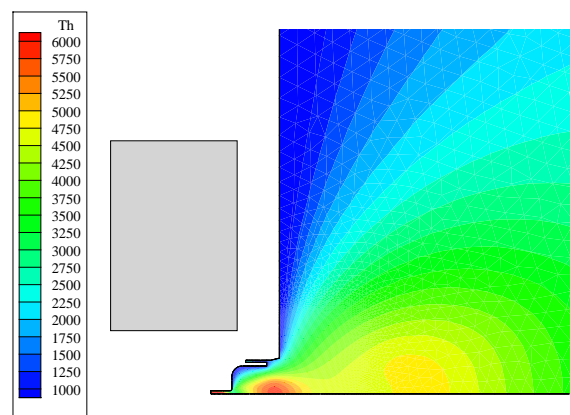
(c) Electron temperature  $T_e$ , no anomalous diffusion included.



(d) Electron temperature  $T_e$ , anomalous diffusion included.

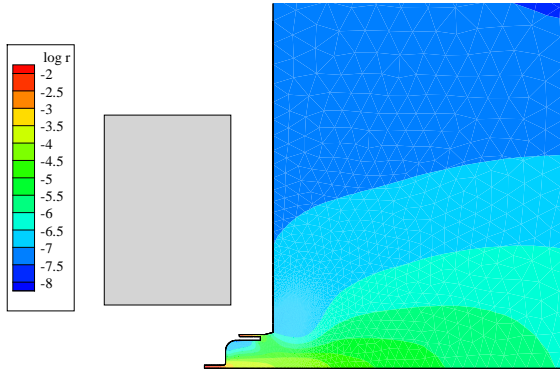


(e) Heavy particle temperature  $T_h$ , no anomalous diffusion included.

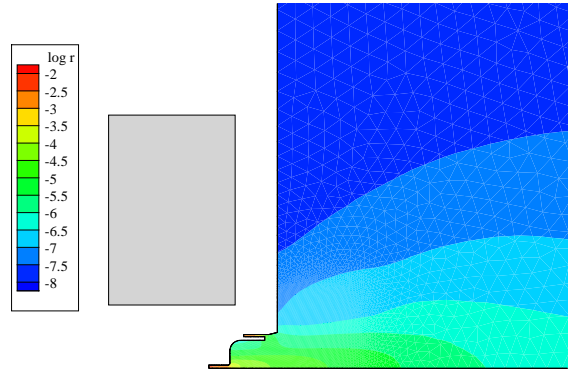


(f) Heavy particle temperature  $T_h$ , anomalous diffusion included.

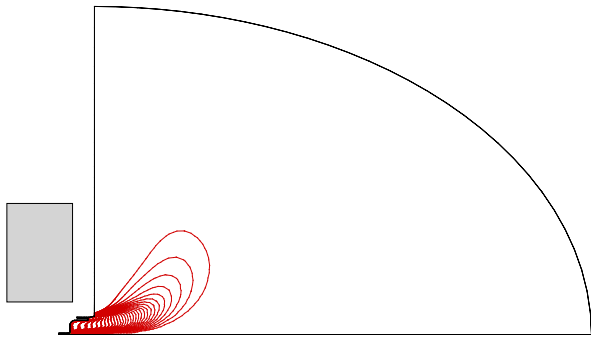
**Figure 2.** Comparison of numerical results for numerical simulation of an AF-MPD thruster with and without inclusion of anomalous diffusion: degree of ionization  $\alpha$ , electron temperature  $T_e$  and heavy particle temperature  $T_h$ .



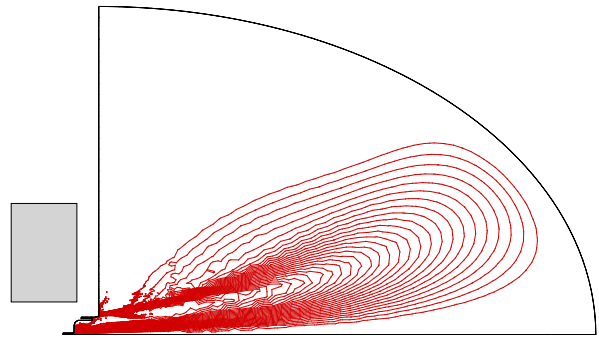
(a) Heavy particle density  $\log_{10} \rho$ , no anomalous diffusion included.



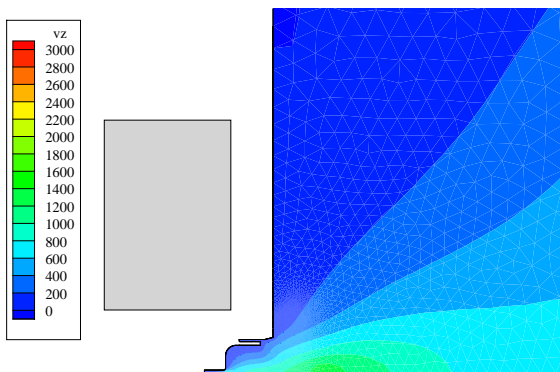
(b) Heavy particle density  $\log_{10} \rho$ , anomalous diffusion included.



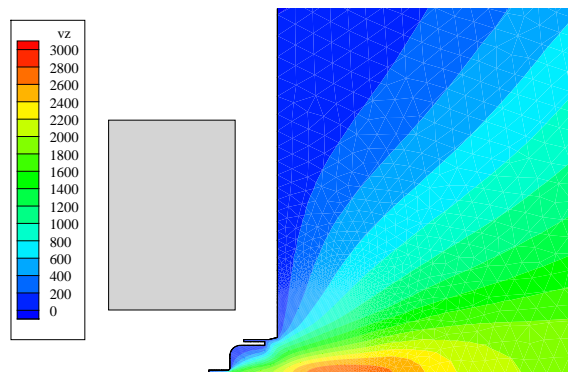
(c) Current distribution  $\Psi$ , no anomalous diffusion included.



(d) Current distribution  $\Psi$ , anomalous diffusion included.



(e) Axial velocity  $v_z$ , no anomalous diffusion included.



(f) Axial velocity  $v_z$ , anomalous diffusion included.

Figure 3. Comparison of numerical results for numerical simulation of an AF-MPD thruster with and without inclusion of anomalous diffusion: current distribution  $\Psi$  and axial velocity  $v_z$ .